Correction: 11 October 2017

www.sciencemag.org/content/357/6358/1406/suppl/DC1

Supplementary Materials for

Gating of social reward by oxytocin in the ventral tegmental area

Lin W. Hung, Sophie Neuner,* Jai S. Polepalli,* Kevin T. Beier,* Matthew Wright, Jessica J. Walsh, Eastman M. Lewis, Liqun Luo, Karl Deisseroth, Gül Dölen, Robert C. Malenka†

*These authors contributed equally to this work.
†Corresponding author. Email: malenka@stanford.edu

Published 29 September 2017, *Science* **357**, 1406 (2017)
DOI: 10.1126/science.aan4994

This PDF file includes:

Correction: Owing to an oversight, the manuscript failed to cite an important study by Song and co-workers that showed that activation of oxytocin receptors in the ventral tegmental area of male Syrian hamsters is essential for the reward-like properties of social interactions. The PDF and HTML versions of the paper have been corrected to cite this reference [now reference (*7*)]. References in this PDF file have been renumbered accordingly.

Supplemental Materials

Material and Methods

Animals

Male C57Bl/6 mice (Jackson Laboratory; stock # 00664) and the following transgenic lines were used: Oxt$^{tm1.1(cre)Dolsn}$/J (*OXTiresCre*, gift from Bradford Lowell, Jackson Laboratory stock #:023234) (*10*); Avp$^{tm1.1(cre)Hze}$/J (*AVPiresCre*, Jackson Laboratory stock #:023530) (*28*); Oxtr$^{tm1.1Wsy}$/J homozygous (conditional OXTR knockout, Jackson Laboratory stock #:008471) (*13*); Oxtr$^{tm2.1Knis}$ (OXTr-Venus, gift from Larry Young, MGI:3838764) (*12*); Slc6a3$^{tm1.1(cre)bkmn}$/J (*DATCre*; Jackson Laboratory stock #: 006660) (*29*); Gad2$^{tm2(cre)Zjh}$/J (*GAD2Cre*; Jackson Laboratory stock #: 010802) (*30*); Gt(ROSA)26Sor$^{tm14(CAG-tdTomato)Hze}$/J (Ai14; Jackson Laboratory stock #: 007908) (*31*). All mice were kept on a C57Bl/6 background and were housed on a 12-hour light/dark cycle with food and water ad libitum. All behavioral experiments were conducted during the same circadian period (7:00-19:00). All procedures compiled with animal care standards set forth by the National Institute of Health and were approved by Stanford University's Administrative Panel on Laboratory Animal Care and Administrative Panel of Biosafety.

Stereotactic injections and optic fiber cannula implantations

Stereotactic injections of viruses and retrobeads were performed under general ketamine-medetomidine anesthesia using a stereotactic instrument. A small volume of concentrated virus solution (500 nL) or diluted (1:5) retrobeads (300 nL) was injected into the target regions at a slow rate (125 nL/min) using a syringe pump. The injection needle was withdrawn 5 min after the end of the infusion. The accurate location of injection sites and viral infectivity were confirmed in all mice post-hoc by preparing sections (50 µm) containing the relevant brain regions. Adeno-associated viruses (AAV) used in this study were purchased from the Stanford Neuroscience Gene Vector and Virus Core and included: AAV_{DJ}-CMV-DIO-Kir2.1-ZsGreen, AAV_{DJ}-CMV-DIO-Zsgreen, AAV_{DJ}-CAG-DIO-eGFP-Cre, AAV_{DJ}-efl α-DIO-Cheta-eYFP, AAV_{DJ}-ef1α-DIO-NphR3.0-eYFP, AAV_{DJ}-efl α-DIO-eYFP, AAV_{DJ}-eflα-DIO-GCaMP6m and AAV_{DJ}-eflα-DIO-GCaMP6m. AAV titers ranged from 3.8 X 10^{12} to 1.7 X 10^{13} gc/ml. CAV2-Cre was purchased from E. Kremer (Institut de Génétique Moléculaire de Montpellier, France). For experiments involving analysis or manipulation of cell bodies, we waited for at least 4 weeks

following virus injections. For experiments involving analysis or manipulation of axon terminals, we waited at least 8 weeks.

For optogenetic behavioral experiments, mice received bilateral implantations of optic fiber cannulas. Cannulas were made in-house using 1.25 mm diameter multimode ceramic ferrule, 200 µm fiber optic cable with NA 0.39 and blue dye epoxy. Cannulas were secured to the skull using miniature screws (thread size 00-90 x 1/16) and light-cured dental adhesive cement. The incision was closed with a tissue adhesive

For injections and cannula placements, coordinates for specific brain regions were as follows: PVN (bregma - 0.75 mm; lateral 1.5 mm at a 15 degrees-angle; ventral 4.9 mm); VTA (bregma -3.2 mm, lateral 1.25 mm at 10 degrees-angle; ventral 4.35 mm), NAcMedS (bregma +1.9 mm; lateral 0.7 mm; ventral -4.1 mm).

Social Conditioned Place Preference (sCPP)

The sCPP protocol was adapted from (*4*). Animals were weaned at 3 weeks of age into "home" cages containing 3-5 cage-mates and housed on corncob bedding (0.125 inches). Any requisite surgeries were performed at P28. At P35, animals were placed in open field activity chamber equipped with infrared beams and a software interface that monitors the position of the mouse. The apparatus was partitioned into two equally sized zones using a clear Plexiglas wall, with a 5-cm diameter circular hole at the base; each zone contained one type of novel bedding (crumpled paper; soft granule). The amount of time spent freely exploring each zone was recorded during 30-min test sessions. After an initial pre-conditioning trial (pre-test) to establish baseline preference for the two sets of bedding cues, mice were assigned to receive social conditioning with cage mates for 24 hours on the bedding type in which they spent less time. Mice that exhibited >70% preference for one bedding type during the pre-test were excluded from further conditioning. After social conditioning, mice were then housed in the other type of bedding alone without cage mates. Twenty-four hours later, mice received a 30-min post conditioning trial (post-test). For individual experimental conditions, post-test versus pre-test preference scores were compared using a paired student's t-test with $P < 0.05$ considered significant. Comparisons between experimental conditions were made using normalized scores (post-test time spent in social bedding zone/pre-test time in social bedding zone) and were considered significant if unpaired student's t-test P values were < 0.05.

Cocaine Conditioned Place Preference (cocaine CPP)

For cocaine CPP, experiments were performed in the same open field activity chambers as sCPP except that each chamber was divided into two equally sized zones using plastic floor tiles with distinct visual and tactile cues (grey and smooth or clear and rough). After 5 days of daily saline injections in the home cage, the amount of time spent freely exploring each zone (divided by a clear Plexiglass wall with a 5 cm dimeter circular hole at the base) was recorded during a 30 min pre-test session. Over the next 2 days, 24 hours apart, mice received either an injection of cocaine (20 mg/kg) or saline (equal volumes) in a counterbalanced fashion and were immediately placed in one of the two different zones in which they were restricted by a Plexiglass wall (without any opening). A 30 min post-test preference session was conducted 24 hours after the second conditioning session during which mice were free to explore both zones (divided by the Plexiglass wall with the open circular hole at the base). Analyses were conducted and significance determined as for social CPP.

Real-Time Conditioned Place Preference (RT-CPP)

The RT-CPP protocol was conducted as described previously (*32*) in a rectangular Plexiglas cage with 3 chambers separated by removable Plexiglass walls. The left and right chambers each measured 28 cm X 24 cm and had distinct wall patterns (black and white stripes versus black and white squares) and flooring (smooth versus rough plastic floors). The center chamber measured 11.5 cm x 24 cm with no wall patterns and a smooth clear floor. For the RT-CPP assay, an experimental mouse was placed in the center compartment for 2 min at which point the barriers were lifted and the mouse was allowed to freely explore the entire apparatus for 15 minutes during which it was photostimulated whenever it entered the designated chamber, which was alternated between each testing session. Video tracking software recorded all animal movements and automatically analyzed time spent and distance moved in each chamber. Preference was calculated as percentage of time spent in the photostimulated side of the chamber (i.e. [time in photostimulated side / (time in photostimulated side + time in non-photostimulated side)] X 100.)

For optogenetic photostimulation the cannulas were connected to a 473 nm laser diode through a FC/PC adaptor and a fiber optic 1X2 rotary joint. Laser output was controlled using a pulse stimulator, which delivered 5 ms light pulses at 30 Hz. Light output through the optical fibers was adjusted to ~25 mWatts using a digital power meter console. For activation of

NpHR3.0, the optical fiber was connected to a 532 nm laser diode via a FC/PC adaptor and a fiber optic 1X2 rotary joint. Laser output was again controlled using a pulse stimulator, on a 8 seconds on and 2 seconds off cycle. Light output was adjusted to ~10 mWatts.

Social Real Time Conditioned Place Preference

The sRT-CPP protocol was a modified version of the RT-CPP assay. On day 1, mice were placed for 15 min in the 3 chamber apparatus that contained a conspecific juvenile (male, 3-5 weeks) under a cage in one of the two side chambers. On day 2, the experimental mice were again exposed to the same juvenile on the same side of the three-chamber box but were photostimulated whenever they entered the chamber containing the juvenile in a manner identical to that done for RT-CPP. Video tracking software recorded all animal movements and automatically analyzed time spent and distance moved in each chamber. Preference was calculated as time spent in social chamber on day 1 subtracted from time spent on day 2.

3-chamber sociability test

This assay was conducted as described previously (*33*). A day prior to the experimental session, mice were habituated to the 3 chamber apparatus for 5 min. On the test day, a conspecific juvenile (male, 3-5 weeks) was placed under a cage in one of the large side chambers and an empty cage was placed in the other side chamber. Experimental mice were then placed in the center chamber for 2 minutes before the barriers were lifted at which point mice were allowed to freely explore for 10 min. Experimental mice were then removed from the apparatus at which time a novel conspecific juvenile was placed under the previously empty cage. The experimental mice were then placed back in the center chamber with barriers in place. Within 60 sec, barriers were then lifted and experimental mice were allowed to freely explore the three chambers for a further 10 minutes as a test of "social memory". During optogenetic experiments, constant photostimulation occurred for the duration of both the sociability and social memory sessions. Location of mice was again assayed automatically using the Cleversys Topscan software. Sociability was calculated as a percentage of time spent in the side of the chamber containing the juvenile mouse ([time in juvenile side / (time in juvenile side + time in empty side)] X 100.). Social recall was calculated as a percentage of time spent in the side of the chamber containing the novel juvenile mouse ([time in novel juvenile side / (time in novel juvenile side + time in familiar juvenile side)] X 100.).

Juvenile Interaction Test

Juvenile interaction in the home cage was conducted as described previously (*8*). Briefly, cagemates were temporarily moved to a holding container and the test animal connected to the fiber-optic patch cord and returned to its home cage with the lid removed for 2 minutes. A conspecific juvenile mouse (male, 3-5 weeks) or a toy mouse was then placed in the home cage for 5 min during which free interactions were allowed. All sessions were video recorded and analyzed in real time. Social contact behavior was considered to occur when the test mouse moved at a velocity above threshold (35 mm/s) and approached either the juvenile or toy mouse within a distance of 10 mm.

During optogenetic activation experiments, mice were photostimulated with a 473 nm laser diode using one of two different photostimulation protocols. For constant stimulation, 30 Hz pulses (5 ms pulse width with a power output of ~25 mWatts) were delivered continuously for the entire 5 min duration of the experiment. For context-dependent stimulation, experimental mice were stimulated at 30 Hz whenever they were within 2 cm of either the juvenile or toy mouse. Stimulation was triggered using animal tracking software and a data acquisition module. For optogenetic inhibition experiments using NpHR3.0, mice were photostimulated with 532 mm laser diodes (power output at ~10 mWatts on a 8 seconds on and 2 seconds off cycle) either continuously for the duration of the experiment (constant stimulation) or when experimental mice were within 2 cm of the juvenile or toy mouse (context-dependent stimulation).

Fiber Photometry

OXTiresCre mice were injected with AAV_{DJ}-eflα-DIO-GCaMP6m into the PVN and a mono fiber-optic cannula (400 µm core diameter; 430 µm outer diameter; 0.48 NA) was implanted at the same coordinates. Fiber photometry was performed as in (*34*). 490 nm LED and 405 nm LEDs were sinusoidally modulated at 531 hz and 211 hz respectively to allow for separation of calcium dependent (490 nm) and independent (405 nm, the isosbestic wavelength of GCaMPm) fluorescence via lock-in amplification at the modulated frequency. The 490 nm light was passed through a GFP excitation filter and the 405 nm light through a 405 nm bandpass filter and both light streams were coupled into the same patch cord (400 um core diameter; 430 um outer diameter; 0.48 NA), which was mated, to the implanted fiber-optic cannula. Emitted GCaMP6f fluorescence was collected by the implanted fiber, passed through a GFP emission

filter, and detected using a photoreceiver. The LEDs were controlled by a real-time signal processor using custom software which also demodulated the fluorescence intensity due to 405 nm and 490 nm excitation. Calcium dynamics were recorded while mice were in their home cage for 2 minutes before and 10 minutes after the addition of a juvenile or toy mouse.

To correct for calcium independent changes in fluorescence, a least-squares linear fit was applied to the 405 nm calcium independent signal to align it to the 490 nm calcium dependent signal, and this aligned fit was subtracted from the 490 nm signal to yield calcium dependent GCaMP fluorescence as in (*35*). The baseline was further corrected by subtracting the 8th percentile of dF/F over a rolling 20s window to correct for photobleaching and other longer time-scale noise. Time-locked transients were determined by converting dF/F to z score for each animal and subtracting the median fluorescence during the 1s before each event to normalize the baseline for each event to zero similar to (*36*). These time-locked z scores were then averaged for each event type to generate average transients. For juvenile interactions, 25 individual events were averaged from 6 mice with a range of 1-7 per mouse. For toy mouse interactions 26 events were averaged from 4 mice with a range of 1-16 per mouse.

Immunohistochemistry

Animals were transcardially perfused with 4% paraformaldehyde (PFA) or 10% formalin and then further post-fixed overnight with coronal sections (50 µM) prepared on a vibratome in PBS. Sections were blocked with 10% normal donkey serum (NDS) and 2% bovine serum albumin (BSA) in PBS/0.5% triton-X100 (PBST), then stained for OXT (gift from Harold Gainer; mouse anti-OXT-NP; 1:400), AVP (gift from Harold Gainer; rabbit anti-AVP-NP; 1:1000), TH (rabbit anti-TH; 1:1000; EMD Millipore, USA), GFP (sheep anti-GFP; 1:1000; Novus, USA) **or** c-fos antibody (goat anti-c-fos; 1:1000; Santa Cruz, USA), in 1% NDS in PBST overnight at room temperature (RT). Sections were rinsed three times for 30 minutes each at room temperature, followed by secondary antibody stain (1:200 for all, Alexa Fluor 647 anti-mouse, Alexa Fluor 647 anti-rabbit, Alex Fluor 488 anti-mouse, Alexa Fluor 594 anti-sheep) in 1% NDS in PBT at RT for 3 hours. Sections were then rinsed three times for 30-minutes each, and mounted on slides. Image acquisition was performed with a confocal system using 10X, 40X or 63X objectives. Images were analyzed using ImageJ FIJI software.

For c-fos quantifications in the VTA (Fig. S10), animals were sacrificed 90 minutes after the final optical stimulation at 30 Hz for 30 minutes. Sections were processed as described above

for immunohistochemical staining for c-fos and TH. Sections containing the ventral midbrain were imaged on the Nikon confocal microscope at 20x magnification. Each confocal image was acquired using identical pinhole, gain and laser settings. Images were acquired with a 10-step z-stack at 5 µm intervals. The results from each of the three sections for each brain were averaged for the final results. For c-fos quantifications in the PVN (Fig. 2B), two-month old Ai14 reporter male mice were injected bilaterally with 500 ηL of CAV2-Cre in each VTA (AP: -3.3, ML: -1.1 at 10 degrees; DV: -4.35). After recovering for 2 weeks, mice were exposed to either novel juvenile (of the same strain, less than P35 days old) or toy mice. Mice were sacrificed 90 minutes post-interaction. Tissue was processed as above, except sections containing the PVN were co-stained for c-fos and OXT. Sections were quantified in a similar fashion as for the VTA.

Identification of magnocellular and parvocellular OXT neuronal projections.

At postnatal day 30, 100 nl retrobeads (diluted 1:5) were injected unilaterally into VTA (AP: adjusted for Bregma-Lambda distance (BL) using the following formula; $\left((BL \div 4.2) \times 3.4\right) - 0.4$; ML: -0.3; DV: -4.2 from brain surface). As described previously (*37, 38*), 24 hours prior to transcardial perfusion with 10% formalin, 30 µl 4% Fluoro-Gold was diluted in sterile saline and injected into the lateral tail vein over the course of two injections using a syringe and 25 gauge needle. Animals were perfused 5 days after retrobead injections. Brains were post-fixed overnight, and coronal sections of the PVN (25 µm) and VTA (40 µm) were cut in phosphate buffered saline (PBS) using a vibratome. Sections were mounted on slides in PBS and allowed to dry. Subsequently, sections were rinsed 4 times for 10 min each and blocked with 10% normal horse serum (NHS) and 2% bovine serum albumin (BSA) in PBS/0.5% triton-X100 (PBST). The PVN was stained with OXT (mouse anti-OT-NP, gift of Dr. Harold Gainer; 1:150) and FG (rabbit anti-FG, Fluorochrome;1:100) and the VTA was stained with TH antibody (rabbit anti-TH, Millipore; 1:400), all in 1% NHS in PBST at RT for 4 hours. Sections were rinsed 4 times for 10 min each in PBS at room temperature (RT) followed by 2 hour RT secondary antibody stain using Alexa Fluor 555 anti-mouse and Alexa Fluor 647 anti-rabbit (diluted 1:1000 in 1% NHS in PBST for both). Sections were then rinsed 4 times for 10 min each at RT and slides were cover-slipped. Images were acquired using an Olympus BX 41 microscope with 4x and 40x objectives and Q-Capture Pro 7 software. Subsequently, images were analyzed using ImageJ.

Electrophysiology

Mice were deeply anesthetized with pentobarbital (200 mg/kg intraperitoneally). Coronal midbrain slices (250 μm) were prepared after intracardiac perfusions with ice-cold artificial cerebrospinal fluid (ACSF) containing (in mM): 50 sucrose, 125 NaCl, 25 $NaHCO_3$, 2.5 KCl, 1.25 NaH_2PO_4, 0.1 $CaCl_2$, 4.9 $MgCl_2$ and 2.5 glucose (oxygenated with 95% O_2 and 5% CO_2). After 90 minutes of recovery at 36°C, slices were transferred to a recording chamber and perfused continuously at 2-4 ml/min with oxygenated ACSF (125 NaCl, 25 $NaHCO_3$, 2.5 KCl, 1.25 NaH_2PO_4, 2.5 $CaCl_2$, 1.3 $MgCl_2$ and 11 glucose; osmolarity of ~300) at 30°C. For sequential recording of IPSCs and EPSCs, internal solution contained (in mM) 135 $CeMeSO_4$, 8 NaCl, 2 Mg-ATP, 0.3 Na-GTP, 7 phosphocreatine, 0.25 EGTA, 10 HEPES and 0.1 spermine with a pH 7.24 and 291 osmolarity. Patch pipettes (3.5 – 4.5 MΩ) were pulled from borosilicate glass. Retrobead labeled NAcMedS-projecting dopamine neurons were visualized with a 40X water-immension objective on an upright fluorescent microscope equipped with an infrared-differential interface contrast video microscopy and epifluorescence for detection of green retrobeads and tdTomato in DA neurons.

EPSCs and IPSCs were evoked by placing a bipolar theta glass stimulating electrode within the VTA. PSCs were recorded in whole-cell voltage clamp, filtered at 4 kHz, digitized at 8 kHz and acquired online. VTA DA neurons were voltage-clamped at -60 mV for EPSCs and 0 mV for IPSCs. For pharmacological characterization, electrically evoked EPSCs and IPSCs were recorded for 5 minutes followed by bath application of 1 μM TGOT for 10 minutes and then washed out with 1 μM OXTrA for a further 10 minutes. To measure the membrane properties, we used an internal solution containing (in mM) 135 $KMeSO_4$, 17 HCl, 20 HEPES, 0.2 EGTA, 2.8 NaCl, 5 Mg-ATP and 0.5 Na-GTP with a pH of 7.2. Firing properties were measured by injecting an incremental step current of 25pA for 500ms, starting from -100pA. Spontaneous spiking in VTA DA neurons was acquired in voltage clamp cell-attached configuration. Briefly, baseline firing was acquired for 5 minutes, followed by bath application of drugs for 5-10 min, followed by a 15-20 min washout of the drug. For the analysis of spontaneous spiking, the spiking frequency was calculated for 30 s intervals and normalized to baseline.

Blinding and Statistics

For virtually all behavioral experiments in this study, investigators were blinded to the treatment condition of the experimental mice and during the data acquisition, data analyses and

outcome assessments. Specifically, these blinded conditions applied to experiments shown in Fig.'s 1, 2B, 2I-P, 3, S1, S3 – S8. As stated in figure legends, Student's two-tailed t-tests were used to compare two groups. Multiple groups were compared using one-way ANOVA with Dunnett's post hoc test. For comparing manipulations over time, a two-way ANOVA was performed with Bonferroni's multiple comparison post-hoc test used for more than 2 groups.

Supplementary Figures

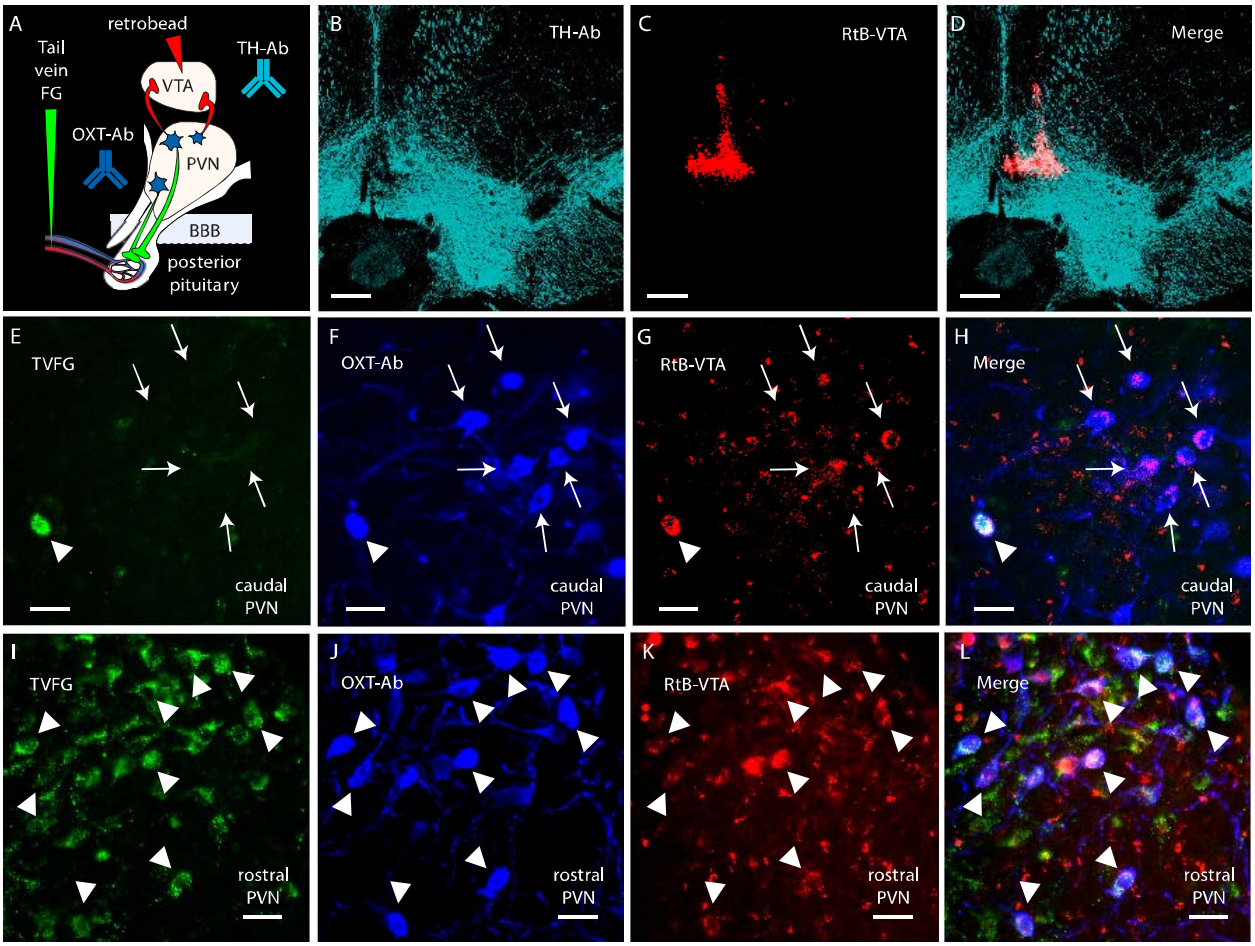

Fig. S1. VTA receives both magnocellular and parvocellular OXT neuronal projections from the PVN. (A) Diagram illustrating injection strategy. Retrobeads (RtB) were injected into the ventral tegmental area (VTA), and the blood-brain barrier impermeant retrograde tracer Fluoro-Gold (FG) was injected into the tail vein (TV) of the same animals to label paraventricular nucleus (PVN) neurons. Tyrosine Hydroxylase (TH), Oxytocin (OXT), and FG were detected by antibody labeling in the VTA or PVN. **(B)** TH labeling at the RtB injection site in the VTA. **(C)** VTA retrobead injection. **(D)** Merge of the images shown in B and C. **(E)** FG labeling in the caudal PVN. **(F)** OXT neurons in the same section. **(G)** RtB labeling in the same section. **(H)** Merge of the images shown in E-G. At this level of the PVN, most OXT neurons are unlabeled by FG, indicating that they are parvocellular. **(I)** FG labeling in the rostral PVN. **(J)** OXT neurons in the same section. **(K)** RtB labeling. **(L)** Merge of the images shown in I-K. At this level of the PVN, most OXT neurons are labeled by FG, indicating that they are magnocellular. Arrowheads indicate VTA-projecting magnocellular OXT neurons, and arrows indicate parvocellular VTA-projecting OXT neurons. Scale bars represent 250 µm in low magnification images (B-D) and 25 µm in high magnification images (E-L).

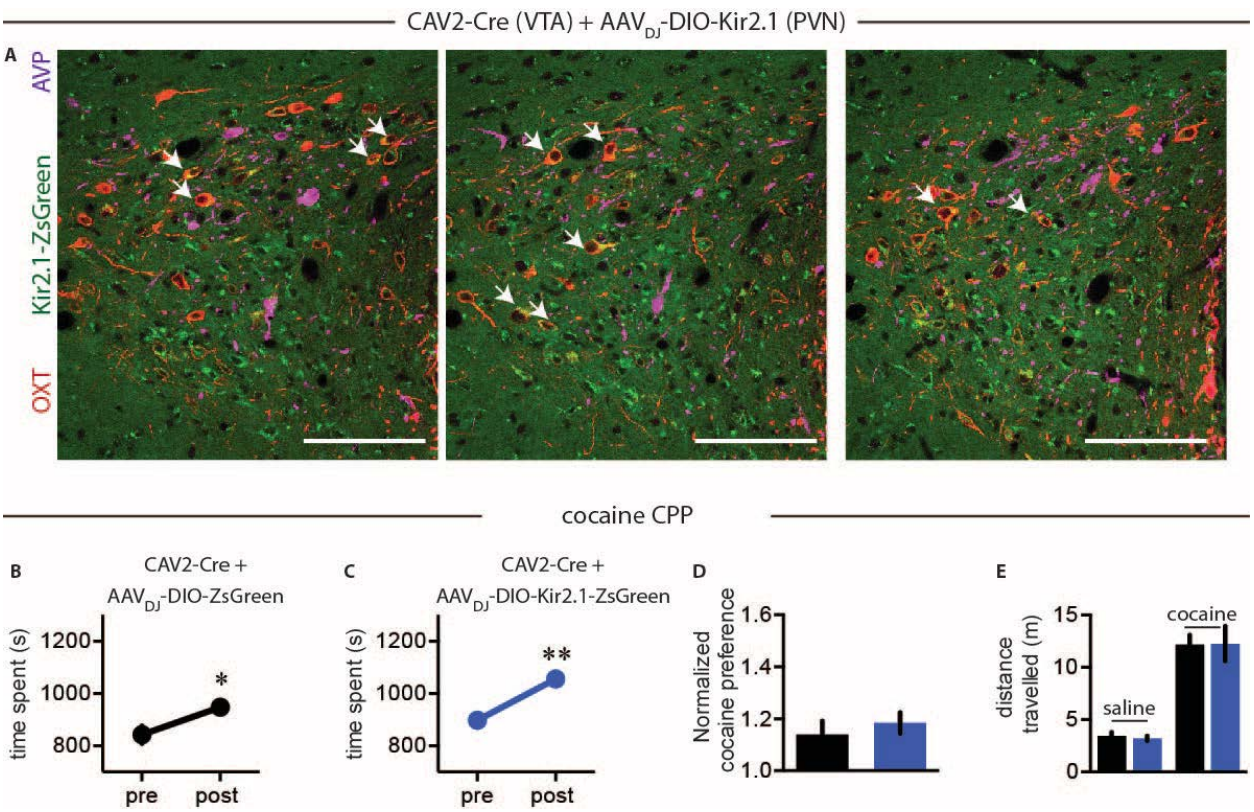

Fig. S2. Silencing of PVN projections to VTA does not affect cocaine CPP. (A) Immunohistochemical images showing co-localization of Kir2.1-ZsGreen (green) primarily with OXT neurons (red) but not AVP neurons (magenta) in the PVN**.** Scale bar, 100 µm. **(B-D)** Quantification of cocaine CPP for control mice expressing ZsGreen (B) or mice expressing Kir2.1-ZsGreen (C) in PVN neurons projecting to the VTA (n = 10 for both groups). Normalized cocaine preference is shown in D. **(E)** Graphs showing distance travelled during these tests. Data represent mean ± SEM. Significance was calculated by means of paired *t*-test for within group comparison (B & C) and unpaired *t*-test for across group comparison (D & E). ** $P < 0.01$. Comparisons with no asterisk had $P > 0.05$ and were not considered significant.

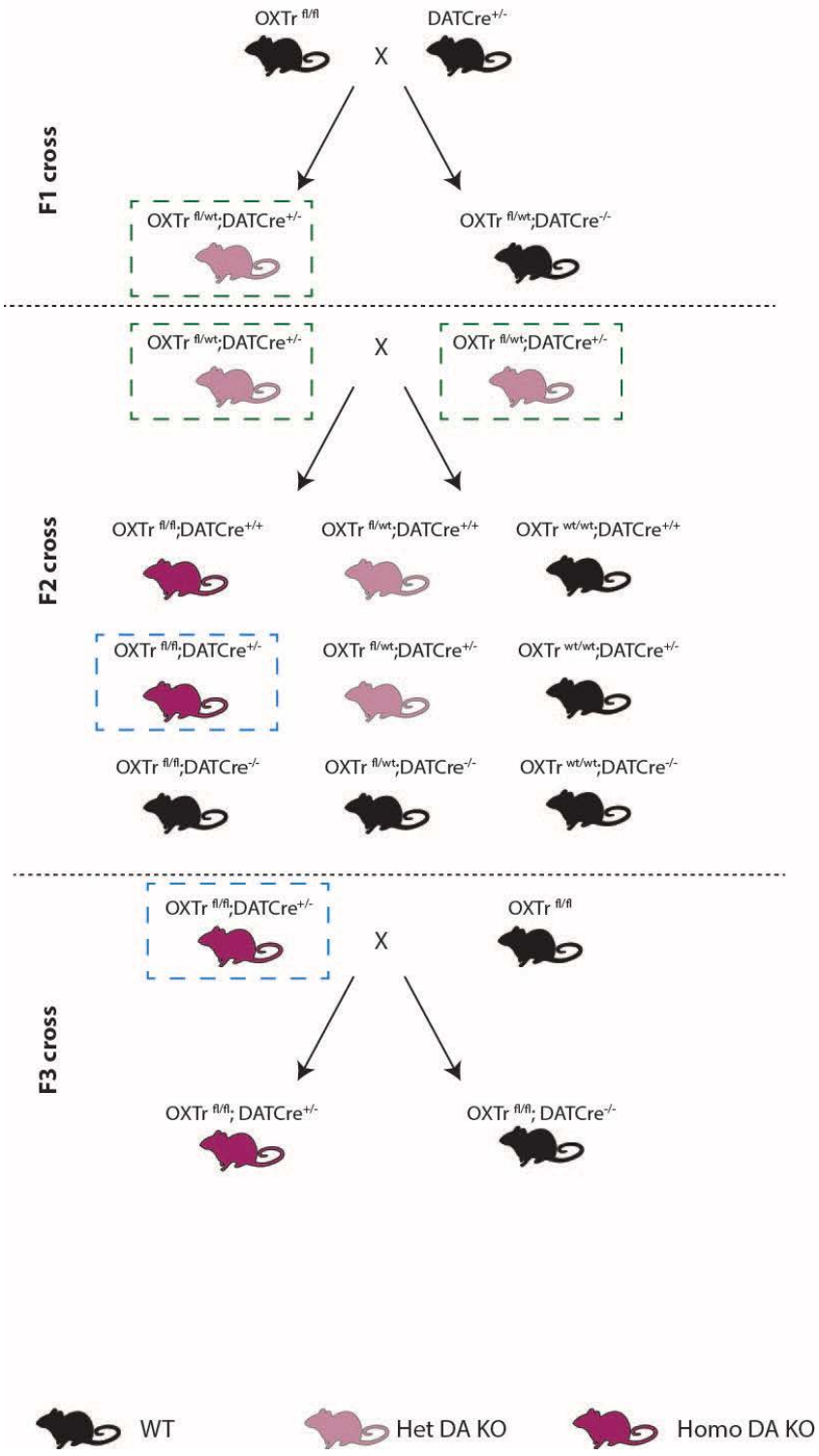

Fig. S3 Breeding strategy to obtain homozygous knock out (KO) of OXTr in DA neurons. DA neuron specific OXTr KOs were generated by first crossing DATCre$^{+/-}$ mice with homozygous OXTr$^{fl/fl}$ mice. Heterozygous KOs from two separate breeding pairs (in green dashed boxes) were then crossed with each other. The final F3 cross generated littermates that were OXTr$^{fl/fl}$ with no Cre present (WT) and homozygous OXTr KOs in DA neurons (Homo DA KO) This breeding scheme was replicated to create specific OXTr KOs from GABA neurons by using GAD2Cre$^{+/-}$ mice instead of DATCre$^{+/-}$ mice.

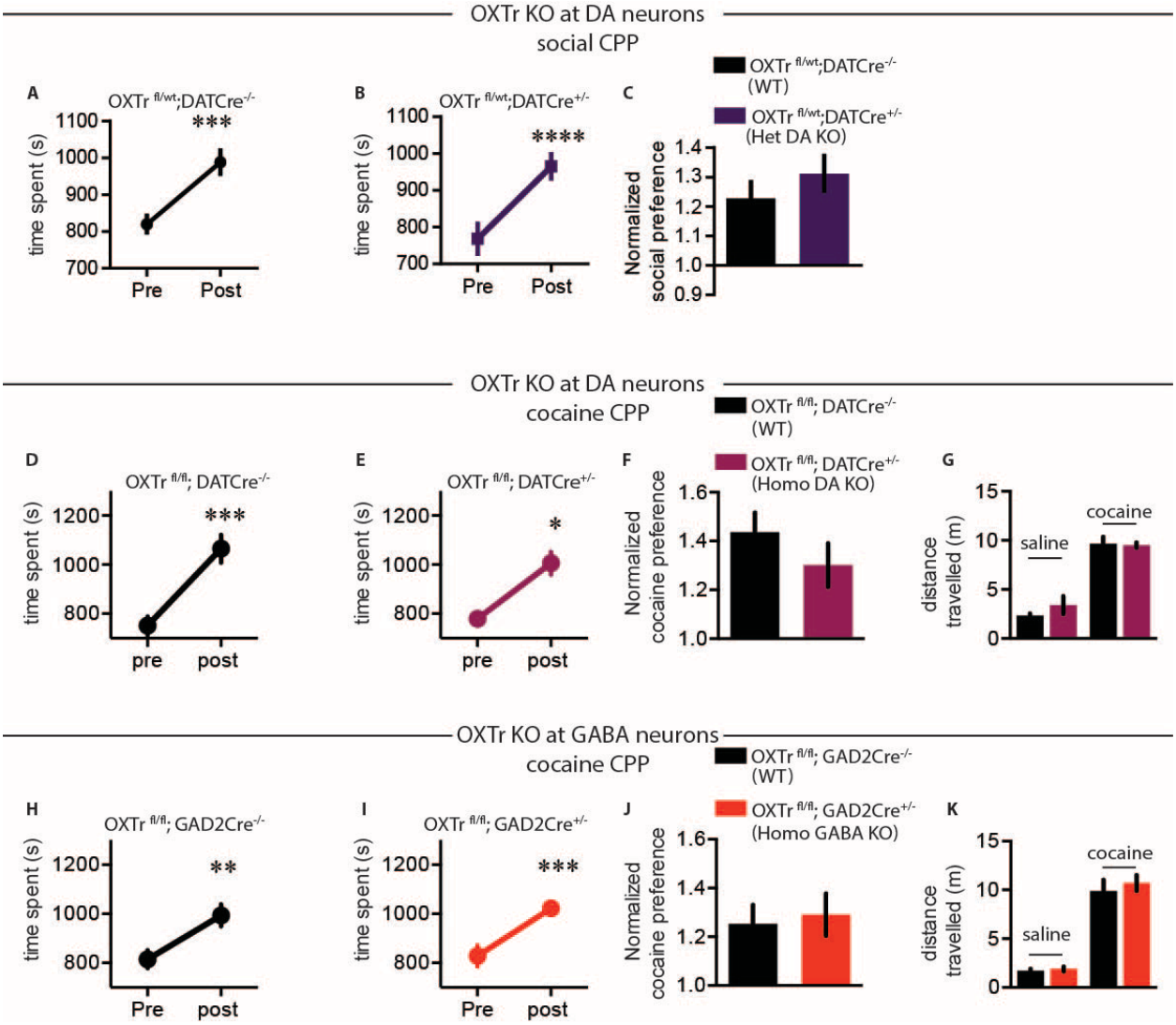

Fig. S4 Mice with heterozygous OXTr KO in DA neurons display normal social CPP while homozygous OXTr KO in DA or GABA neurons display normal cocaine CPP. (A-C) Quantification of social CPP in WT (n = 17) or heterozygous OXTr DA KO (n = 20) mice. **(D–F)** Quantification of cocaine CPP for WT (n = 10) or homozygous OXTr DA KO (n=5). **(G)** Distance travelled during cocaine CPP conditioning**. (H-J)** Quantification of cocaine CPP for WT (n = 14) or homozygous OXTr GABA KO (n = 15). **(K)** Distance travelled during cocaine CPP conditioning. Data represent mean ± SEM. Significance was calculated by means of paired *t*-test for within group comparison (A, B, D, E, H, & I) and unpaired *t*-test for across group comparison (C, F, G, J & K). * $P < 0.05$, ** $P < 0.01$, *** $P < 0.001$. Comparisons with no asterisk had $P > 0.05$ and were not considered significant.

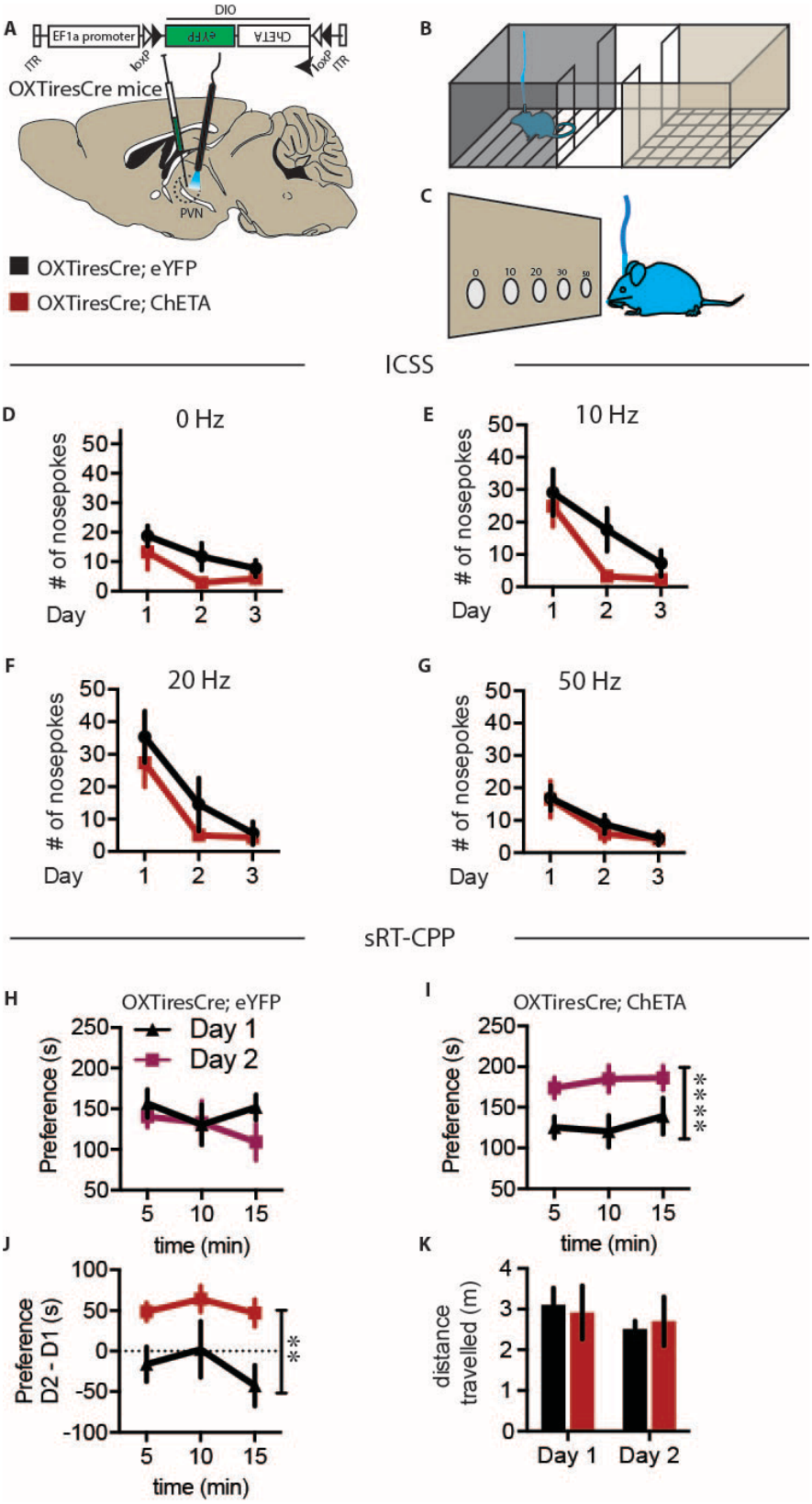

Fig. S5. PVN OXT neuronal activation does not induce instrumental learning but enhances sRT-CPP. (A) Schematic showing somatic opto-genetic photostimulation of PVN OXT neurons; **(B)** RT-CPP experimental set-up; **(C)** ICSS using nose pokes in different holes to elicit optogenetic stimula-tion at different frequen-cies. **(D-G)** Quantification of nose pokes in control eYFP and ChETA expressing mice for the holes that elicited 0, 10, 20 or 50 Hz stimulation (n = 8 for each group). **(H-J)** Time spent on the social side of the chamber (preference) for Day 1 and Day 2 for eYFP and ChETA expressing mice (n = 10 for each group). Mice received photostimulation on Day 2. (**J**) Subtracted preferences (Day 2-Day 1) for eYFP (black) and ChETA (red) expressing mice. **(K)** Distance travelled by eYFP and ChETA mice during sRT-CPP for both days. Data represent mean ± SEM. Significance was calcu-lated by means of two-way ANOVA for **(**H - J). ** P < 0.01, **** P < 0.0001. Comparisons with no asterisk had P > 0.05 and were not considered significant.

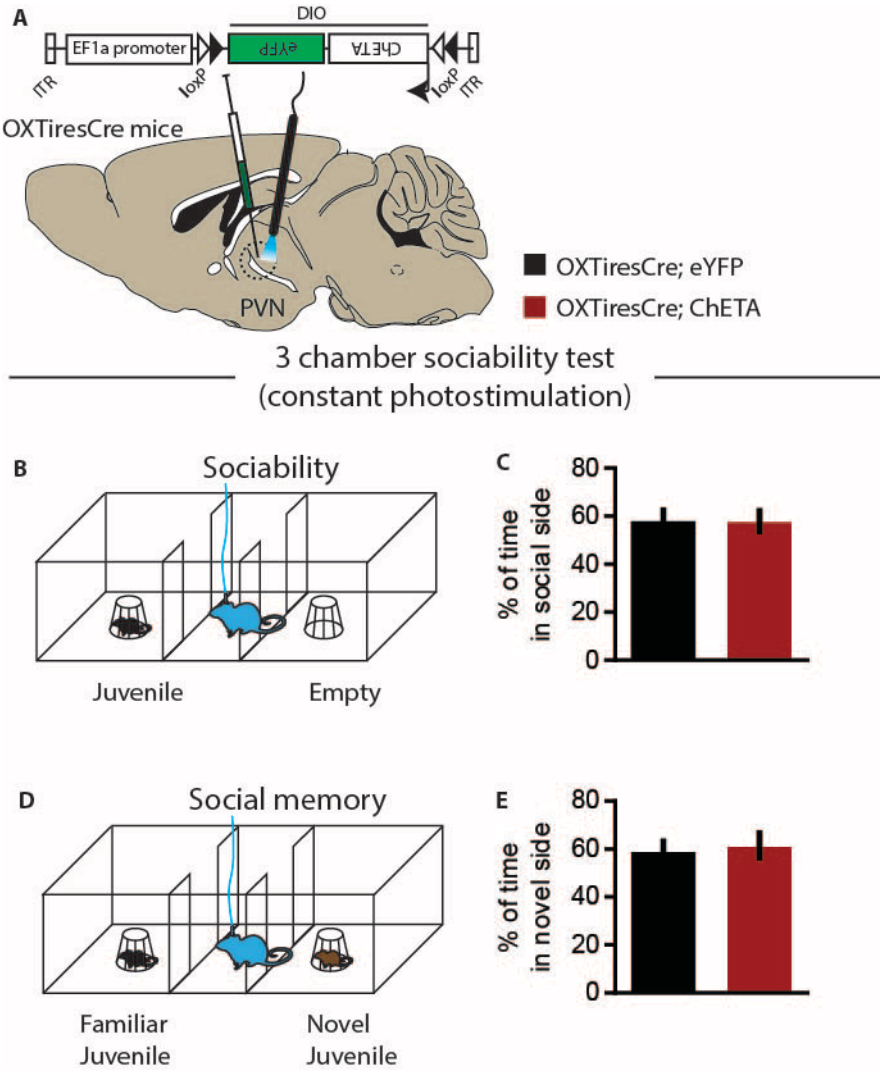

Fig. S6. Constant PVN OXT neuronal activation does not affect sociability nor social memory. (A) OXTiresCre mice were injected with AAVDJ-DIO-ChETA-eYFP or AAVDJ-DIO-eYFP and a fiber optic was placed in the PVN. (**B**) Schematic showing that mice were subjected to a three-chamber sociability test during which they received constant photostimulation for duration of experiment (10 min). **(C)** Graph showing the percentage of time spent on social chamber (n = 8 and 6 for YFP and ChETA groups, respectively). **(D)** Schematic showing setup for social memory assay during which a new novel juvenile was placed in a cage on the side that previously had an empty cage and the same mice were immediately tested. **(E)** Graph showing percentage of time spent on the side of the box containing the novel juvenile. Data represent mean ± SEM. Significance was calculated by means of unpaired *t*-test for across group comparison (C&E). No asterisk indicates $P > 0.05$, which was considered not significant.

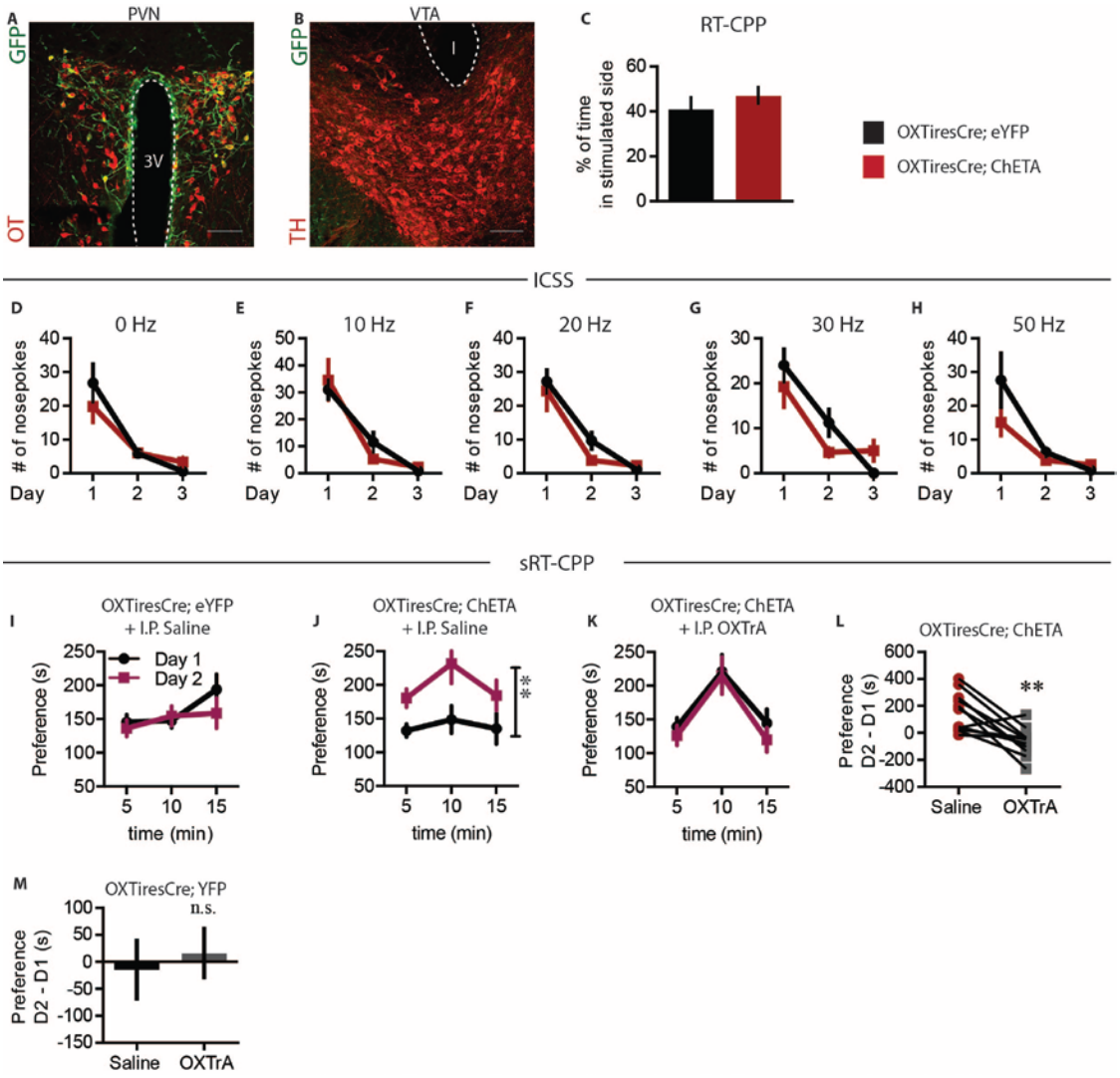

Fig. S7. Optogenetic activation of OXT axons/terminals in VTA does not induce instrumental learning. Immunohistological images showing: **(A)** co-localization of GFP (green) and OXT (red) cells in the PVN and **(B)** fiber placement in the VTA (TH neurons in red). Scale bar, 100 µm. **(C)** Quantification of RT-CPP experiments showing percentage of time spent in the stimulated side (n = 8 and 14 for YFP and ChETA groups, respectively). **(D-H)** Quantification of ICSS showing the number of nose pokes mice performed to receive photostimulation at different frequencies (n = 8 and 12 for YFP and ChETA groups, respectively). **(I, J)** Quantification of preference for social side during sRT-CPP assay on Day 1 and Day 2, on which animals received photostimulation in VTA as well as saline injections i.p. (n = 7 and 12 for YFP and ChETA mice, respectively). (**K**) Quantification of preference for social side as in J except the same ChETA mice received I.P injection of OXTrA (5 mg/kg, n = 12). Saline and OXTrA experiments were performed in two different sRT-CPP sessions separated by 1 week with treatments interleaved to avoid order effects. **(L)** Subtracted preference values (Day 2-Day 1) for each ChETA mouse following saline (J) or OXTrA (K) administration. (**M**) OXTrA administration did not affect baseline preference in eYFP control mice. Data represent mean ± SEM. Significance was calculated by means of paired *t*-test (L), unpaired *t*-test (C, M), or two-way ANOVA (I - K). ** $P < 0.01$. Comparisons with no asterisk had $P > 0.05$ and were not considered significant.

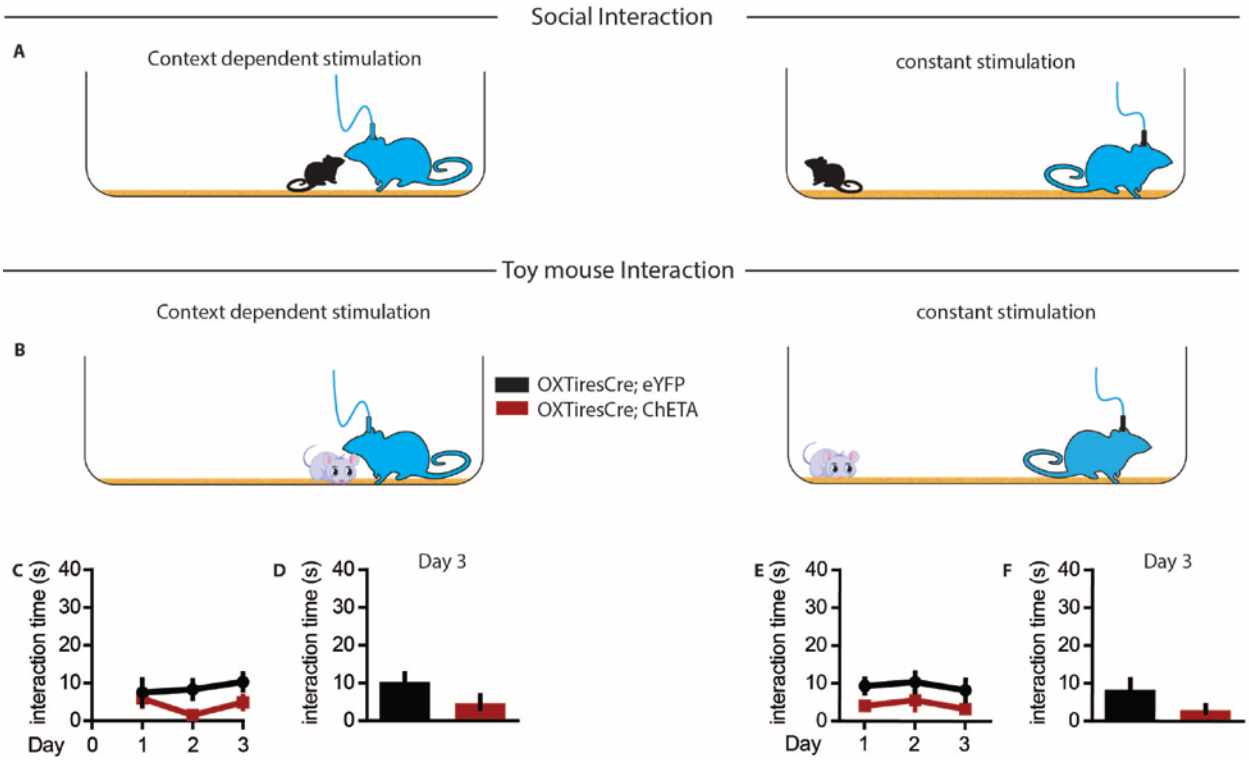

Fig. S8. Activation of OXT axons/terminals in the VTA does not affect interaction with toy mouse. Schematic of **(A)** juvenile or **(B)** toy interaction experiments where photostimulation occurred in a context-dependent or constant manner. Mice had either eYFP alone or ChETA expressed in PVN OT neurons. **(C)** Quantification of time spent interacting with toy mouse during context dependent stimulation over 3 days. (**D**) Interaction time on Day 3. **(E)** Quantification of time spent interacting with toy mouse during constant photostimulation. (**F**) Interaction time on Day 3 (n = 8 for both groups). Data represent mean ± SEM. Significance was calculated by means of unpaired *t*-test for across group comparison (D, F). No asterisk indicates $P > 0.05$ and was not considered significant.

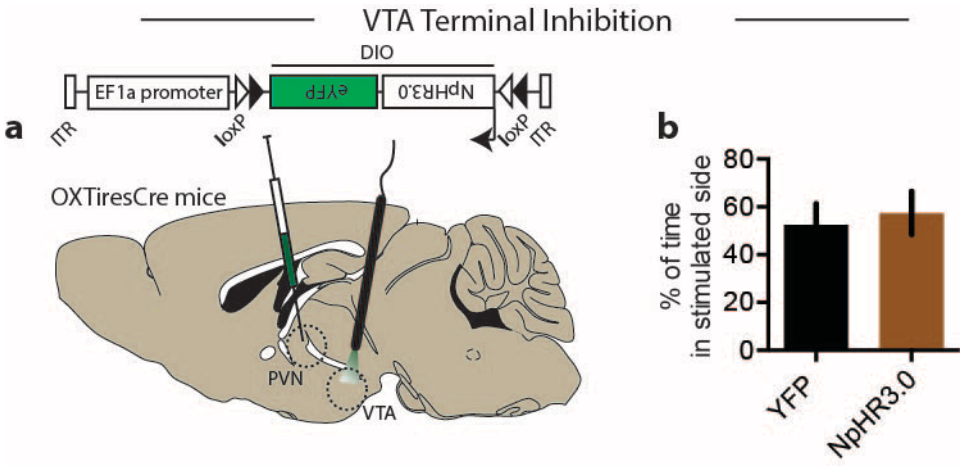

Fig. S9. Optogenetic inhibition of OXT fibers in the VTA does not elicit any changes in RT-CPP. (A) Schematic showing OXTiresCre mice with AAV_{DJ}-DIO-NpHR3.0-eYFP injected in the PVN and fibers implanted at the VTA. **(B)** Quantification of percentage of time spent in the stimulated side for YFP and NpHR3.0 expressing mice (n = 7 for both groups). Data represent mean ± SEM. Significance was calculated by means of unpaired *t*-test. No asterisk indicates $P > 0.05$ and was not considered significant.

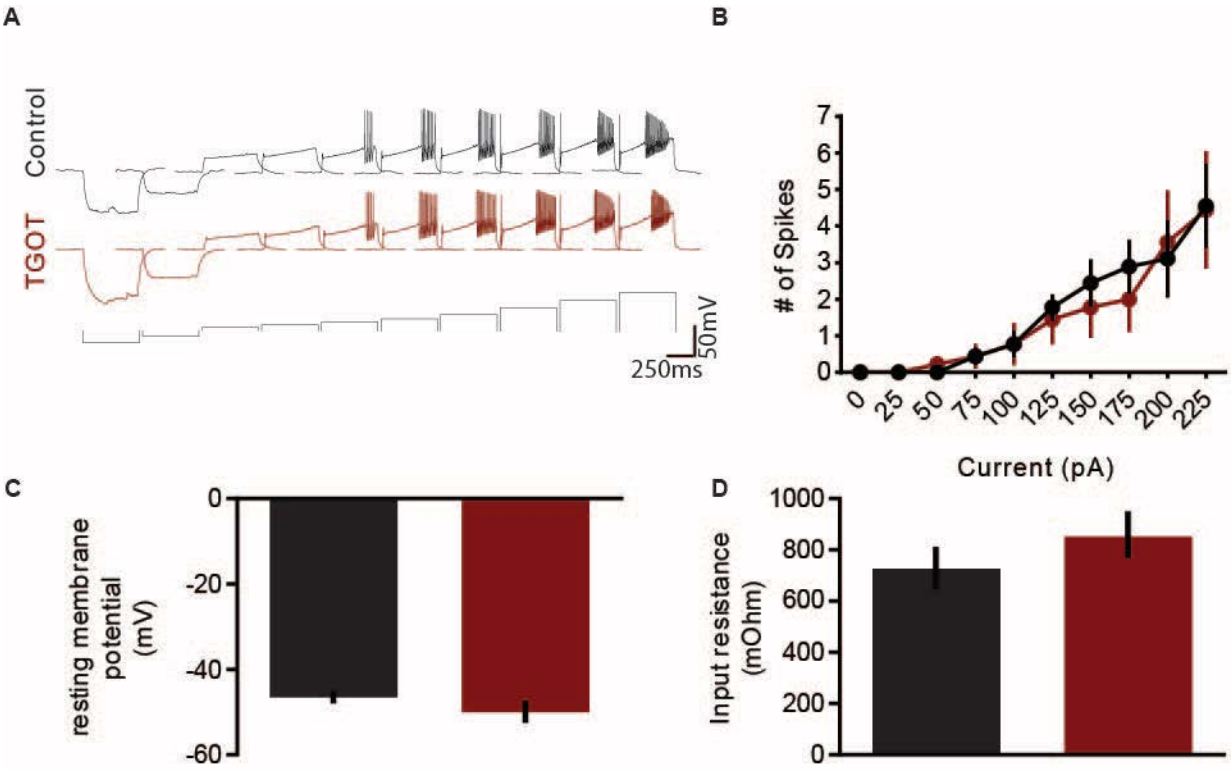

Fig. S10. Effect of TGOT on the membrane properties of NAcMedS projecting VTA DA neurons. (A) Sample traces for NAcMedS projecting VTA DA neurons in response to a series of hyperpolarizing and depolarizing current pulses. **(B)** Summary graph showing effect of TGOT on the excitability of neurons in response to varying current injections. Resting membrane potentials (**C**) and input resistances **(D)** were unchanged by TGOT application (n = 10 for both groups). Data represent mean ± SEM. Significance was calculated by means of unpaired *t*-test for across group comparison (C, D). No asterisk indicates $P > 0.05$ and was considered not significant.

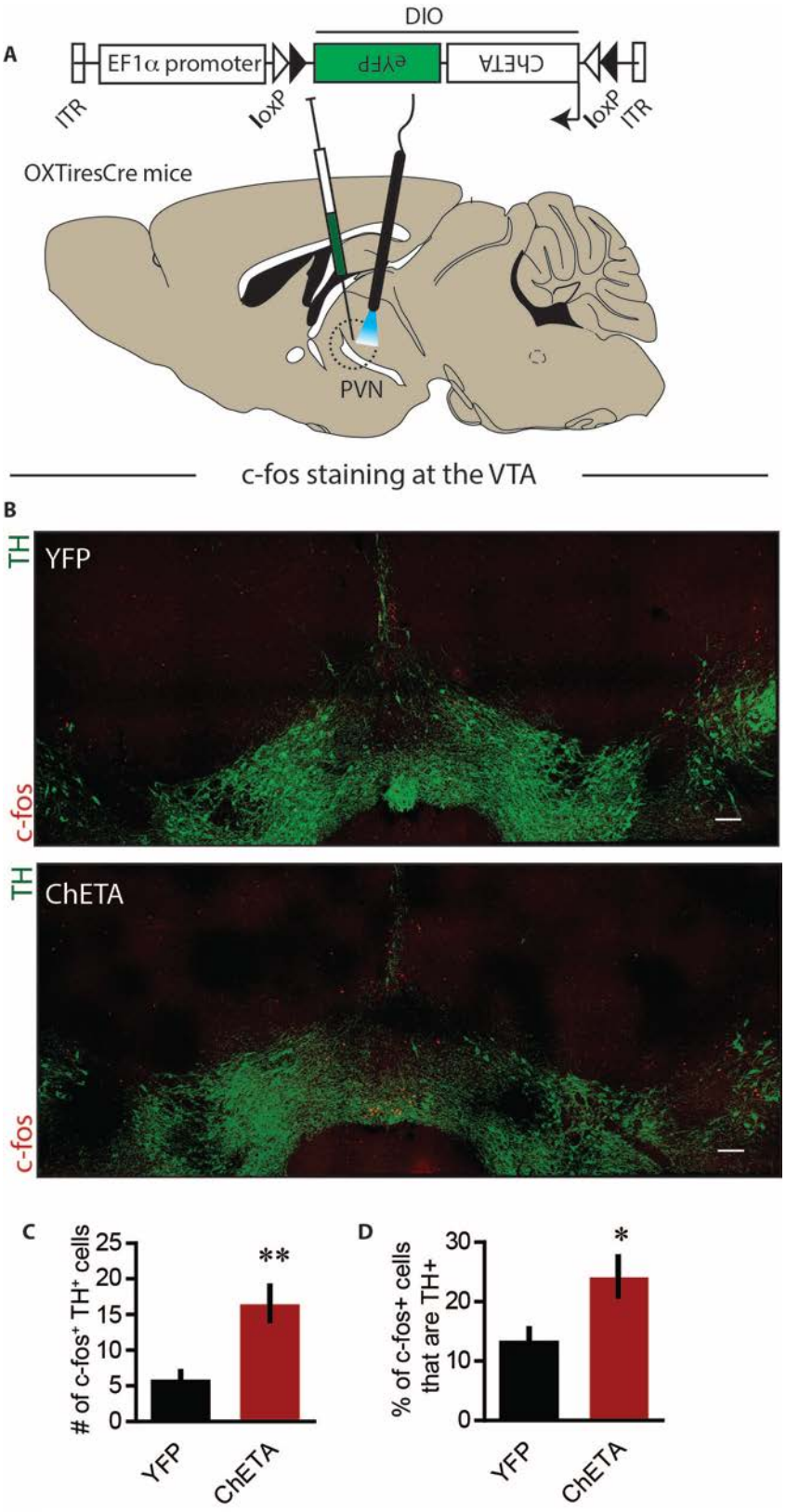

Fig. S11. VTA neurons are activated upon activation of PVN OXT neurons. (A) Schematic showing injection of AAV_{DJ}-DIO-ChETA-eYFP or AAV_{DJ}-DIO–eYFP into the PVN of OXTiresCre mice and placement of optical fiber. (**B**) Immunohistochemical images showing co-localization of TH (green) and c-fos (red) cells in the VTA of OXTiresCre mice expressing YFP or ChETA in the PVN of OXTiresCRE mice.. Scale bar, 100 µm. (**C**) Quantification of the number of c-fos positive cells that are also TH positive following photostimulation of PVN OXT neurons (n = 7 and 9 for YFP and ChETA groups, respectively). (**D**) Percentage of c-fos positive cells that are TH positive. Data represent mean ± SEM. Significance was calculated by means of unpaired *t*-test for across group comparison. * $P < 0.05$, ** $P < 0.01$.

References and Notes

1. C. Chevallier, G. Kohls, V. Troiani, E. S. Brodkin, R. T. Schultz, The social motivation theory of autism. *Trends Cogn. Sci.* **16**, 231–239 (2012). doi:10.1016/j.tics.2012.02.007 Medline

2. L. J. Young, C. E. Barrett, Can oxytocin treat autism? *Science* **347**, 825–826 (2015). doi:10.1126/science.aaa8120 Medline

3. L. J. Young, Z. Wang, The neurobiology of pair bonding. *Nat. Neurosci.* **7**, 1048–1054 (2004). doi:10.1038/nn1327 Medline

4. G. Dölen, A. Darvishzadeh, K. W. Huang, R. C. Malenka, Social reward requires coordinated activity of nucleus accumbens oxytocin and serotonin. *Nature* **501**, 179–184 (2013). doi:10.1038/nature12518 Medline

5. S. A. Buffington, G. V. Di Prisco, T. A. Auchtung, N. J. Ajami, J. F. Petrosino, M. Costa-Mattioli, Microbial reconstitution reverses maternal diet-induced social and synaptic deficits in offspring. *Cell* **165**, 1762–1775 (2016). doi:10.1016/j.cell.2016.06.001 Medline

6. S. G. Shamay-Tsoory, A. Abu-Akel, The social salience hypothesis of oxytocin. *Biol. Psychiatry* **79**, 194–202 (2016). doi:10.1016/j.biopsych.2015.07.020 Medline

7. Z. Song, J. M. Borland, T. E. Larkin, M. O'Malley, H. E. Albers, Activation of oxytocin receptors, but not arginine-vasopressin V1a receptors, in the ventral tegmental area of male Syrian hamsters is essential for the reward-like properties of social interactions. *Psychoneuroendocrinology* **74**, 164–172 (2016).

8. L. A. Gunaydin, L. Grosenick, J. C. Finkelstein, I. V. Kauvar, L. E. Fenno, A. Adhikari, S. Lammel, J. J. Mirzabekov, R. D. Airan, K. A. Zalocusky, K. M. Tye, P. Anikeeva, R. C. Malenka, K. Deisseroth, Natural neural projection dynamics underlying social behavior. *Cell* **157**, 1535–1551 (2014). doi:10.1016/j.cell.2014.05.017 Medline

9. S. Lammel, B. K. Lim, R. C. Malenka, Reward and aversion in a heterogeneous midbrain dopamine system. *Neuropharmacology* **76**, 351–359 (2014). doi:10.1016/j.neuropharm.2013.03.019 Medline

10. K. T. Beier, E. E. Steinberg, K. E. DeLoach, S. Xie, K. Miyamichi, L. Schwarz, X. J. Gao, E. J. Kremer, R. C. Malenka, L. Luo, Circuit architecture of VTA dopamine neurons revealed by systematic input-output mapping. *Cell* **162**, 622–634 (2015). doi:10.1016/j.cell.2015.07.015 Medline

11. Z. Wu, Y. Xu, Y. Zhu, A. K. Sutton, R. Zhao, B. B. Lowell, D. P. Olson, Q. Tong, An obligate role of oxytocin neurons in diet induced energy expenditure. *PLOS ONE* **7**, e45167 (2012). doi:10.1371/journal.pone.0045167 Medline

12. M. Yoshida, Y. Takayanagi, K. Inoue, T. Kimura, L. J. Young, T. Onaka, K. Nishimori, Evidence that oxytocin exerts anxiolytic effects via oxytocin receptor expressed in serotonergic neurons in mice. *J. Neurosci.* **29**, 2259–2271 (2009). doi:10.1523/JNEUROSCI.5593-08.2009 Medline

13. H. J. Lee, H. K. Caldwell, A. H. Macbeth, S. G. Tolu, W. S. Young 3rd, A conditional knockout mouse line of the oxytocin receptor. *Endocrinology* **149**, 3256–3263 (2008). doi:10.1210/en.2007-1710 Medline

14. S. Lammel, E. E. Steinberg, C. Földy, N. R. Wall, K. Beier, L. Luo, R. C. Malenka, Diversity of transgenic mouse models for selective targeting of midbrain dopamine neurons. *Neuron* **85**, 429–438 (2015). doi:10.1016/j.neuron.2014.12.036 Medline

15. K. Schilling, D. Luk, J. I. Morgan, T. Curran, Regulation of a fos-lacZ fusion gene: A paradigm for quantitative analysis of stimulus-transcription coupling. *Proc. Natl. Acad. Sci. U.S.A.* **88**, 5665–5669 (1991). doi:10.1073/pnas.88.13.5665 Medline

16. H. K. Choe, M. D. Reed, N. Benavidez, D. Montgomery, N. Soares, Y. S. Yim, G. B. Choi, Oxytocin mediates entrainment of sensory stimuli to social cues of opposing valence. *Neuron* **87**, 152–163 (2015). doi:10.1016/j.neuron.2015.06.022 Medline

17. J. N. Ferguson, L. J. Young, E. F. Hearn, M. M. Matzuk, T. R. Insel, J. T. Winslow, Social amnesia in mice lacking the oxytocin gene. *Nat. Genet.* **25**, 284–288 (2000). doi:10.1038/77040 Medline

18. J. P. Burkett, E. Andari, Z. V. Johnson, D. C. Curry, F. B. M. de Waal, L. J. Young, Oxytocin-dependent consolation behavior in rodents. *Science* **351**, 375–378 (2016). doi:10.1126/science.aac4785 Medline

19. H. S. Knobloch, A. Charlet, L. C. Hoffmann, M. Eliava, S. Khrulev, A. H. Cetin, P. Osten, M. K. Schwarz, P. H. Seeburg, R. Stoop, V. Grinevich, Evoked axonal oxytocin release in the central amygdala attenuates fear response. *Neuron* **73**, 553–566 (2012). doi:10.1016/j.neuron.2011.11.030 Medline

20. J. Marlin, M. Mitre, J. A. D'amour, M. V. Chao, R. C. Froemke, Oxytocin enables maternal behaviour by balancing cortical inhibition. *Nature* **520**, 499–504 (2015). doi:10.1038/nature14402 Medline

21. L. L. Oettl, N. Ravi, M. Schneider, M. F. Scheller, P. Schneider, M. Mitre, M. da Silva Gouveia, R. C. Froemke, M. V. Chao, W. S. Young, A. Meyer-Lindenberg, V. Grinevich, R. Shusterman, W. Kelsch, Oxytocin enhances social recognition by modulating cortical control of early olfactory processing. *Neuron* **90**, 609–621 (2016). doi:10.1016/j.neuron.2016.03.033 Medline

22. S. F. Owen, S. N. Tuncdemir, P. L. Bader, N. N. Tirko, G. Fishell, R. W. Tsien, Oxytocin enhances hippocampal spike transmission by modulating fast-spiking interneurons. *Nature* **500**, 458–462 (2013). doi:10.1038/nature12330 Medline

23. S. E. Groppe, A. Gossen, L. Rademacher, A. Hahn, L. Westphal, G. Gründer, K. N. Spreckelmeyer, Oxytocin influences processing of socially relevant cues in the ventral tegmental area of the human brain. *Biol. Psychiatry* **74**, 172–179 (2013). doi:10.1016/j.biopsych.2012.12.023 Medline

24. Y. Paloyelis, O. M. Doyle, F. O. Zelaya, S. Maltezos, S. C. Williams, A. Fotopoulou, M. A. Howard, A spatiotemporal profile of in vivo cerebral blood flow changes following intranasal oxytocin in humans. *Biol. Psychiatry* **79**, 693–705 (2016). doi:10.1016/j.biopsych.2014.10.005 Medline

25. O. Peñagarikano, M. T. Lázaro, X.-H. Lu, A. Gordon, H. Dong, H. A. Lam, E. Peles, N. T. Maidment, N. P. Murphy, X. W. Yang, P. Golshani, D. H. Geschwind, Exogenous and evoked oxytocin restores social behavior in the *Cntnap2* mouse model of autism. *Sci. Transl. Med.* **7**, 271ra8 (2015). doi:10.1126/scitranslmed.3010257 Medline

26. E. J. Nestler, S. E. Hyman, Animal models of neuropsychiatric disorders. *Nat. Neurosci.* **13**, 1161–1169 (2010). doi:10.1038/nn.2647 Medline

27. L. Xiao, M. F. Priest, J. Nasenbeny, T. Lu, Y. Kozorovitskiy, Biased oxytocinergic modulation of midbrain dopamine systems. *Neuron* **95**, 368–384.e5 (2017). doi:10.1016/j.neuron.2017.06.003 Medline

28. J. A. Harris, K. E. Hirokawa, S. A. Sorensen, H. Gu, M. Mills, L. L. Ng, P. Bohn, M. Mortrud, B. Ouellette, J. Kidney, K. A. Smith, C. Dang, S. Sunkin, A. Bernard, S. W. Oh, L. Madisen, H. Zeng, Anatomical characterization of Cre driver mice for neural circuit mapping and manipulation. *Front. Neural Circuits* **8**, 76 (2014). doi:10.3389/fncir.2014.00076 Medline

29. C. M. Bäckman, N. Malik, Y. Zhang, L. Shan, A. Grinberg, B. J. Hoffer, H. Westphal, A. C. Tomac, Characterization of a mouse strain expressing Cre recombinase from the 3′ untranslated region of the dopamine transporter locus. *Genesis* **44**, 383–390 (2006). doi:10.1002/dvg.20228 Medline

30. H. Taniguchi, M. He, P. Wu, S. Kim, R. Paik, K. Sugino, D. Kvitsiani, Y. Fu, J. Lu, Y. Lin, G. Miyoshi, Y. Shima, G. Fishell, S. B. Nelson, Z. J. Huang, A resource of Cre driver lines for genetic targeting of GABAergic neurons in cerebral cortex. *Neuron* **71**, 995–1013 (2011). doi:10.1016/j.neuron.2011.07.026 Medline

31. L. Madisen, T. A. Zwingman, S. M. Sunkin, S. W. Oh, H. A. Zariwala, H. Gu, L. L. Ng, R. D. Palmiter, M. J. Hawrylycz, A. R. Jones, E. S. Lein, H. Zeng, A robust and high-throughput Cre reporting and characterization system for the whole mouse brain. *Nat. Neurosci.* **13**, 133–140 (2010). doi:10.1038/nn.2467 Medline

32. S. Lammel, B. K. Lim, C. Ran, K. W. Huang, M. J. Betley, K. M. Tye, K. Deisseroth, R. C. Malenka, Input-specific control of reward and aversion in the ventral tegmental area. *Nature* **491**, 212–217 (2012). doi:10.1038/nature11527 Medline

33. O. Kaidanovich-Beilin, T. Lipina, I. Vukobradovic, J. Roder, J. R. Woodgett, Assessment of social interaction behaviors. *J. Vis. Exp.* **2011**, e2473 (2011).

34. T. N. Lerner, C. Shilyansky, T. J. Davidson, K. E. Evans, K. T. Beier, K. A. Zalocusky, A. K. Crow, R. C. Malenka, L. Luo, R. Tomer, K. Deisseroth, Intact-brain analyses reveal distinct information carried by SNc dopamine subcircuits. *Cell* **162**, 635–647 (2015). doi:10.1016/j.cell.2015.07.014 Medline

35. C. K. Kim, S. J. Yang, N. Pichamoorthy, N. P. Young, I. Kauvar, J. H. Jennings, T. N. Lerner, A. Berndt, S. Y. Lee, C. Ramakrishnan, T. J. Davidson, M. Inoue, H. Bito, K. Deisseroth, Simultaneous fast measurement of circuit dynamics at multiple sites across the mammalian brain. *Nat. Methods* **13**, 325–328 (2016). doi:10.1038/nmeth.3770 Medline

36. G. A. Matthews, E. H. Nieh, C. M. Vander Weele, S. A. Halbert, R. V. Pradhan, A. S. Yosafat, G. F. Glober, E. M. Izadmehr, R. E. Thomas, G. D. Lacy, C. P. Wildes, M. A.

Ungless, K. M. Tye, Dorsal raphe dopamine neurons represent the experience of social isolation. *Cell* **164**, 617–631 (2016). doi:10.1016/j.cell.2015.12.040 Medline

37. J. A. Luther, S. S. Daftary, C. Boudaba, G. C. Gould, K. C. Halmos, J. G. Tasker, Neurosecretory and non-neurosecretory parvocellular neurones of the hypothalamic paraventricular nucleus express distinct electrophysiological properties. *J. Neuroendocrinol.* **14**, 929–932 (2002). doi:10.1046/j.1365-2826.2002.00867.x Medline

38. I. Merchenthaler, Neurons with access to the general circulation in the central nervous system of the rat: A retrograde tracing study with fluoro-gold. *Neuroscience* **44**, 655–662 (1991). doi:10.1016/0306-4522(91)90085-3 Medline